Journal of Materials Chemistry A

First-Principles Explorations of the Electrochemical Lithiation Dynamics of a Multilayer Graphene Nanosheet-based Sulfur-Carbon Composite

Journal:	*Journal of Materials Chemistry A*
Manuscript ID	TA-ART-05-2018-004375.R2
Article Type:	Paper
Date Submitted by the Author:	21-Aug-2018
Complete List of Authors:	Perez-Beltran, Saul; Texas AandM University, Chemical Engineering Balbuena, Perla; Texas AandM University, Chemical Engineering

First-Principles Explorations of the Electrochemical Lithiation Dynamics of a Multilayer Graphene Nanosheet-based Sulfur-Carbon Composite

Saul Perez Beltran and Perla B. Balbuena*
Department of Chemical Engineering, Texas A&M University, College Station, TX 77843
*e-mail: balbuena@tamu.edu

Abstract

Graphitized-polymer-based sulfur cathodes have emerged as alternative cathode materials able to overcome many of technical challenges that currently hinder lithium-sulfur (Li-S) batteries from their use in long-term high-energy applications. However, even though graphitized-polymer-based sulfur cathodes can be synthesized through a facile thermal procedure, and there is evidence of sulfur-carbon chemical bonding, little is known about the electrochemical lithiation processes in these structures. So far, no mechanistic study has followed the dynamics of the discharging process, and no theoretical study has addressed why certain Li-S batteries based on graphitized-polymer-based sulfur cathodes have shown an initial discharge capacity higher than the theoretical discharge capacity of sulfur (1672 mAh/g). Here we use *ab initio* molecular dynamics simulations as a tool to follow the electrochemical lithiation processes in a multilayer graphene nanosheet-based sulfur-carbon composite model embedded in a liquid 1,3-dioxolane solvent phase. Our model reproduces the main structural motifs associated with graphitized-polymer-based sulfur cathodes: chemical sulfur-carbon bonding and π-π stacking for the carbon backbone. Our results indicate that sulfur-carbon bonding prevents sulfur from retaining its stable cyclical structure before lithiation yielding a distribution of linear sulfur chains tightly bonded to the carbon backbone. During lithiation, we observe a competing effect for the incoming electrons between the sulfur atoms and the carbon backbone. This effect induces the partial reduction of the carbon backbone leading to accumulation of additional lithium around it, favoring the lithiation process beyond a 2:1 Li:S molar ratio. As a consequence, it also limits the formation of extended Li_2S-like structures as final reduction products. Finally, comparison of the calculated voltage discharge profile of our model shows close agreement with reported experimental voltage profiles based on sulfur/polyacrylonitrile (SPAN) cathodes, with the proposed mechanisms providing a plausible structural explanation for the additional discharge capacity of SPAN-based cathodes compared to the theoretical discharge capacity of sulfur.

Introduction

Lithium-sulfur (Li-S) batteries offer great potential for high-energy applications, such as electric vehicles and smart grids.[1-3] Theoretically, sulfur delivers a specific energy up to 2500 Wh/kg when coupled with lithium metal, which is ten times higher than that of conventional Li-ion batteries, it is available at low-cost, and it causes a low environmental impact.[4-5] However, several issues like the poor sulfur electrical conductivity still challenge the successful commercialization of Li-S batteries, leading to the incomplete sulfur utilization and its irreversible dissolution into the electrolyte in the form of long-chain lithium polysulfides.[1-3, 6] In an effort to overcome these issues, research efforts point to either the physical confinement or the chemical sequestration of sulfur into conductive frameworks, such as metal sulfides-sulfur composites, metal oxides-sulfur composites, and carbon-sulfur composites, among others.[5-9] So far,

physical confinement of sulfur into macro- and mesoporous-carbonaceous structures has shown significant improvement concerning sulfur electrical conductivity and polysulfides trapping; however, experimental measurements indicate that even though the physical encapsulation, sulfur remains in its cyclic elemental state and eventually leaks out of the cathode in the form of long-chain lithium polysulfides (Li PS).[10] Regarding the sulfur encapsulation into microporous carbonaceous structures, cyclic voltammetry measurements suggest hindered formation of long-chain Li PS, which has led to hypothesize that sulfur is no longer in its S_8 cyclic state but rather in the form of short linear chains of two to four atoms due to its confinement into the narrow microscopic porous structure.[11-12] However, no fundamental level explanation has been provided to back up this proposed electrochemistry, and the Li-S battery still fades in the long term even though the possible absence of long-chain lithium PS.

On the other side, the chemical sequestration of sulfur has achieved varying degrees of success.[13-15] Compared to the physical sulfur impregnation into carbonaceous structures, which is performed at the temperature yielding the sulfur lowest viscosity (159.4 °C), the chemical sequestration of sulfur requires of high temperatures (300 °C or above) to promote the covalent bonding of sulfur to a graphitized polymer-based backbone. Examples of this approach are the sulfur-poly(acrylonitrile) composite (SPAN), the PAN/graphene/sulfur composite, and the PPM/PAN/sulfur composite.[13, 16-18] For the case of the SPAN composite, it has been hypothesized that the high temperatures during synthesis allow that part of the added sulfur dehydrogenates the structure (PAN) releasing H_2S, promoting the PAN cyclization into a conjugated π- π system, and allowing the remaining sulfur to covalently bond to the formed carbonaceous backbone in the form of short-chain sulfur species.[13, 16] Electrochemical measurements on Li-S batteries based on graphitized-polymer-based composites have shown improved utilization of active sulfur, extended battery cyclability, and a discharge profile with only one voltage plateau around ~1.5 V,[13, 16] differing from the classical two-step voltage discharge profile observed in Li-S batteries.[19] To explain this particular discharging behavior, it is hypothesized that chemical bonding between sulfur and carbon prevents sulfur aggregation in its stable cyclic 8-membered structure, limiting the formation of long-chain lithium PS, and preventing the dissolution of intermediate lithium PS into the electrolyte where sulfur is assumed to follow an *all in-solid-state* reduction path.[16] However, so far no mechanistic study has followed *in situ* the electrochemical lithiation dynamics of sulfur in cathode structures with sulfur-carbon bonding, which makes harder to explain how sulfur could follow an *all in-solid-state* reduction path even though when the experimental measurements suggest partial cleavage of sulfur-carbon bonds during discharge.[16] Even more, no theoretical study has explained so far why SPAN-based Li-S batteries have reported an initial discharge capacity higher than the theoretical discharge capacity of sulfur,[13, 16] when the cathode structure is the only source, with no any lithium PS or organosulfur compound added to the electrolyte.[20]

Herein, we aimed to a deeper understanding of the sulfur-carbon interaction by performing *ab initio* molecular dynamics calculations (AIMD) on a multilayer graphene nanosheet-based sulfur-carbon composite embedded in a liquid 1,3-dioxolane (DOL) solvent phase, explicitly designed to facilitate the sulfur-carbon bonding throughout the graphene edges (hereafter-called SC composite). From our calculations, we determined that a stronger sulfur-carbon interaction not only contributes to eliminate the sulfur dissociation into the solvent phase but also leads to an alternative *all in-solid-state* sulfur reduction path skipping the formation of long-chain Li-PS, which helps to explain the improved cycling stability in graphitized-polymer-based cathode structures, like the SPAN composite.[13, 16, 20]

Methodology

Computational Details

For the construction of the initial geometries, we used Materials Studio (version 8.00.843) and Vesta (version 3.4.3); whereas for post-processing and visualization purposes we used homemade computational routines and the open visualization tool OVITO (version 2.9.0).

We followed the system stabilization and lithiation dynamics with the AIMD method as implemented in the Vienna Ab Initio Simulation Package VASP (version 5.4.4). All calculations performed with periodic boundary conditions under the NVT ensemble at 300 K, the temperature oscillations controlled with the Nosé mass parameter set to 0.5, and the hydrogen mass changed to the tritium mass to allow a longer time step of 1 fs.[21] The energy cutoff is set to 400 eV, with the Gaussian smearing parameter set to 0.05 eV and the Brillouin zone sampling done with the Monkhorst-Pack method at a k-point sampling density of 1 x 1 x 1. In addition, we used the Perdew-Burke-Ernzerhof approximation (PBE-GGA) for the exchange-correlation functional, and the Projector Augmented Wave Method (PAW) for treating the core-electron dynamics, with the van der Waals corrections included to the Kohn-Sham energy through the DFT-D3 method of Grimme with Becke-Johnson damping.[22-23] All AIMD simulations were at least eight picoseconds (ps) long to allow the system stabilization down to an averaged energy oscillation less than or equal to 0.01 eV/Atom.

Density functional theory optimizations (DFT) were also performed prior to any structural analysis using the corresponding same simulation parameters from the AIMD simulations, whereas the electronic charge calculations were performed using the grid-based Bader analysis proposed by Henkelman and coworkers.[24] The presence of spin polarized states at the zig-zag edges of nanographene has been reported.[25-26] Also the effect of spin polarization on the interlayer interactions [27] was suggested to produce horizontal interlayer displacements. In our simulations, the effects of chemical reactivity given by the undercoordinated sites are evident. To verify how spin polarization would affect our results, we performed calculations with and without spin polarization shown in Table S1 (Supporting Information). The results showed negligible differences in total energy optimizations for three different lithium contents. Therefore we did not consider spin polarization effects throughout this work.

System Details

Our previous classical molecular dynamics studies [28] with a reactive force field showed us that a random mixture of 8-membered sulfur rings and graphene nanosheets stabilizes into an arrangement of multiple multi-layer graphene ensembles covalently bonded with linear sulfur chains of varying length through the edges of the graphene nanosheets. In this work, we used a similar approach for modeling the sulfur-carbon interaction, which promotes covalent bonding between the two species and reproduces a π-π stacking for the carbon backbone as shown below. Figure 1 shows our SC composite model made of a three-layer graphene ensemble with a 61%-wt. sulfur loading, embedded in a liquid phase of DOL molecules packed up to the solvent's density (1.06 g/cm^3) in an 18 x 18 x 18 Å cubic cell. Even though the graphene sheets size, later in this report we show that the nanographene sheets arrange in stable graphite-like layered stack structures throughout all calculations. On the other side, we should mention that we do not conceive our ensemble of graphene nanosheets as a separated isolated structure embedded in the liqui phase, but as a representation of an interconnected nanographene network capable of enhancing the electronic conductivity of sulfur. Other authors have also pointed out that

nanographene networks are essential for future energy storage application due to their high electron conductivity.[29-33]

The solvent was added using the Materials Studio software built-in packing tool. Here we only use DOL molecules even though we acknowledge that the electrolyte is a more complex mixture of solvents, lithium salts, and other additives.[13, 34-35] For this work, we directed our attention to studying only the interaction between the solvent molecules and the SC composite, and its effects on the lithiation electrochemistry and the composite's capabilities for sulfur retention. In the same way, we did not include the effect of doping the carbon structures with nitrogen (existent in PAN for example)[13] because here we are interested only in a better understanding of the sulfur-carbon bonding effects on the sulfur electrochemical lithiation dynamics. Moreover, earlier works have reported no evidence of direct sulfur-nitrogen bonding, but sulfur-carbon-nitrogen bonding instead, arguing that direct sulfur-nitrogen bonding would significantly perturb the π-π stacking of the carbon backbone.[13]

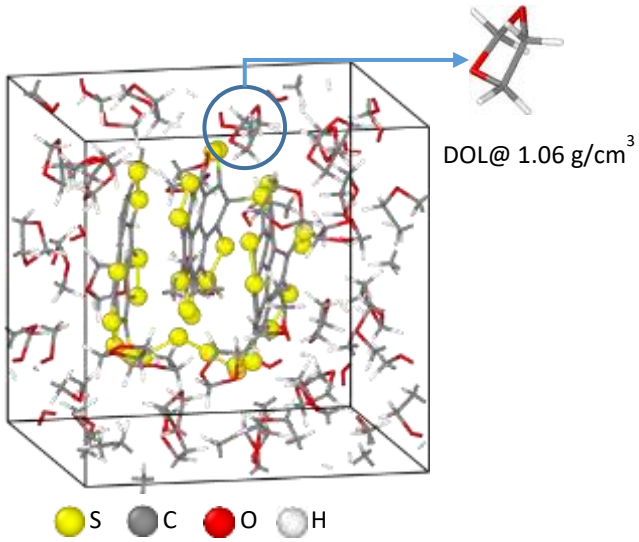

Figure 1: AIMD simulation cell displaying the Sulfur/multi-layer graphene ensemble and surrounding DOL molecules (61-%wt. sulfur loading)

We followed the lithiation dynamics by randomly adding eight lithium atoms nearby the SC composite every eight ps of AIMD simulation, making sure to maintain constant the DOL liquid density even though the increasing lithium content and the limited cell size. Due to the periodic boundary conditions employed, we made small adjustments to the cell size as the number of lithium atoms increased, allowing us to guarantee minimal interactions of the SC composite with its nearby self-images while keeping an acceptable tradeoff between system size and computational cost. Even though the lithium addition rate used here leads to an ionic current significantly higher than the ionic currents reported experimentally elsewhere,[10] eight ps long simulations were long enough to bring the system to stabilization after every Li addition, at which point we did not observe any further reaction taking place. In all AIMD simulations, the maximum energy oscillation was less than or equal to 0.01 eV/Atom in the last two ps of simulations.

Results

AIMD Stabilization of the SC Composite

Figure 2 shows the SC composite after eight ps of AIMD simulation at 300 K, and the radial distribution functions (RDFs) averaged for the last two ps of simulation for the carbon-carbon, carbon-sulfur, and sulfur-sulfur interactions. For the carbon-carbon interaction, the first three peaks at 1.40 Å, 2.48 Å, and 2.86 Å correspond to the first-, second-, and third in plane-coordination spheres between carbon atoms belonging to the same nanosheet. The fourth peak at 3.79 Å corresponds to the separation distance between successive nanosheets, and it locates between the reported interlayer spacing for graphite (3.4 Å) and expanded graphite (4.3 Å),[36-39] suggesting that the carbon backbone of the SC composite holds a π-π stacking configuration even in the presence of solvent molecules. The carbon-sulfur interaction shows a first peak located at 1.745 Å, suggesting chemical bonding between the two species, in agreement with TGA, FTIR, Raman and XPS measurements reported earlier in SPAN composites.[13, 17] Evidence of sulfur-sulfur bonding comes from both the sulfur-sulfur RDF and the structure of SC composite after the eight ps of AIMD simulation. The sulfur-sulfur RDF shows a broad peak centered at 2.1 Å, and the structure of the SC composite complements this information with no evidence of cyclic sulfur structures. Instead, we observe linear sulfur chains of varying length bonded to the graphene nanosheets edges through their terminal sulfur atoms at either or both chain ends. This result is in close agreement with earlier DFT calculations on lithium PS of varying lengths displaying sulfur-sulfur bonding lengths ranging from 2.01 to 2.39 Å depending on the sulfur location within the chain structure.[40-41]

The π-π stacking configuration observed for the carbon backbone, and the different bonding mechanisms suggested from the RDFs analysis closely agrees with the structural characterization proposed to explain the enhanced sulfur retention capabilities of Li-S batteries with graphitized polymer-based sulfur composites like SPAN, PAN/graphene/sulfur, and PMM/PAN/sulfur.[13, 16-18] Moreover, the π-π stacking configuration observed here promotes the formation of a delocalized network of electrons that is thought to improve the electrical conductivity of the SC composite,[42] which contributes to explaining the improved sulfur utilization evidenced during discharge of Li-S batteries based on SPAN-cathodes.[16]

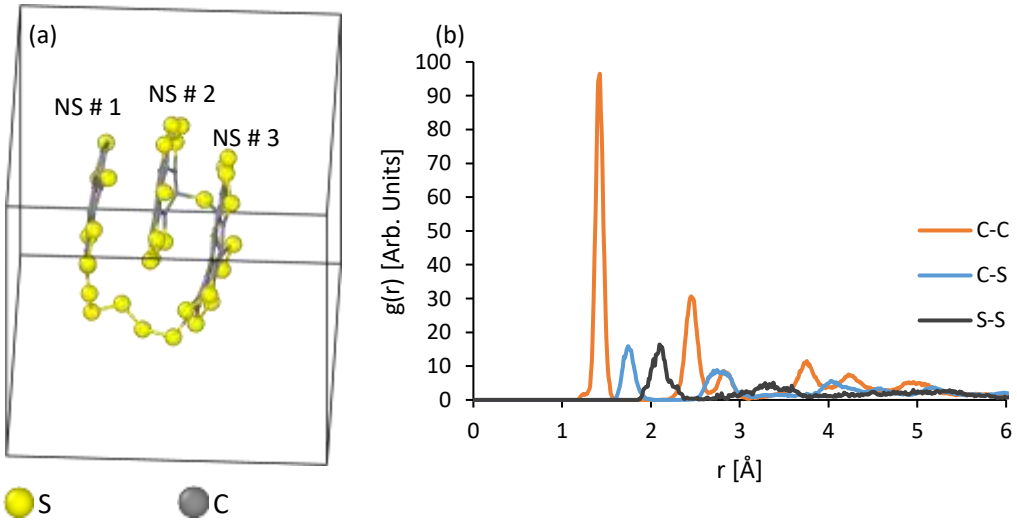

Figure 2: a) SC composite after eight ps AIMD simulation (DOL molecules not shown for clarity), b) RDF pair distribution function.

Table 1 shows the Bader electronic charge distribution of the SC composite and the DOL molecules after the AIMD simulation. For the 40 DOL molecules representing the solvent phase in the simulation cell, we observe an accumulated electronic charge transfer of -0.1163 |e|, which means that each DOL molecule gets a negligible negative charge of -0.003 |e|. Conversely, the SC composite shows an electronic charge depletion of 0.1158 |e|, split between the graphene nanosheets and the sulfur atoms as -2.9317 |e| and 3.0475 |e|, respectively. Although the fractional charges are not observables, and the actual values are a result of the charge estimation procedure, they reflect the calculated electron distribution. The low electronic charge exchange between the solvent phase and the SC composite indicates no interfacial chemical reactions between the DOL molecules and the SC composite at open circuit. On the other hand, the electronic charge transfer from the sulfur atoms to the graphene nanosheets not only confirms the sulfur-carbon chemical bonding but also suggests that the graphene nanosheets might also modify the electrochemical dynamics of sulfur during lithiation, as we discuss later.

Table 1: Calculated electronic charge distribution at open circuit conditions

Structure	**Total electronic charge |e|**
DOL phase	-0.1163
SC composite	0.1158
Sulfur atoms	3.0475
Graphene nanosheets	-2.9317

Figure 3 shows a more detailed view of the electronic charge distribution in one of the graphene nanosheets of the SC composite (NS # 1). The colored mapping of the Bader electronic charge shows that the sulfur atoms bonded to the nanosheet edges contribute the most to the electronic transfer towards the graphene nanosheets, with little to no contribution from the sulfur atoms exclusively involved in sulfur-sulfur interactions. Moreover, Figure 3 also shows the electronic charge transfer between the graphene nanosheets and the sulfur atoms, calculated based on the Equation 1 by subtracting the graphene ($\rho_{Graphene\ nanosheets}$) and sulfur electron densities (ρ_{Sulfur}) from the entire SC composite ($\rho_{SC\ composite}$),[43] with the cyan and yellow isosurfaces representing the electronic density accumulation and depletion, respectively. Further evidence of the sulfur-carbon chemical bonding comes from the charge accumulation at the nanosheets edges with a significant increase between the carbon and sulfur atoms separated a distance centered around 1.745 Å, in agreement with earlier TOF-SIMS and FT-IR measurements in SPAN composites, indicating the existence of sulfur-carbon chemical bonding with no evidence of sulfur in its orthorhombic S_8 state.[13, 16]

$$\Delta\rho = \rho_{SC\ composite} - \rho_{Graphene\ nanosheets} - \rho_{Sulfur} \qquad \text{Eq. 1}$$

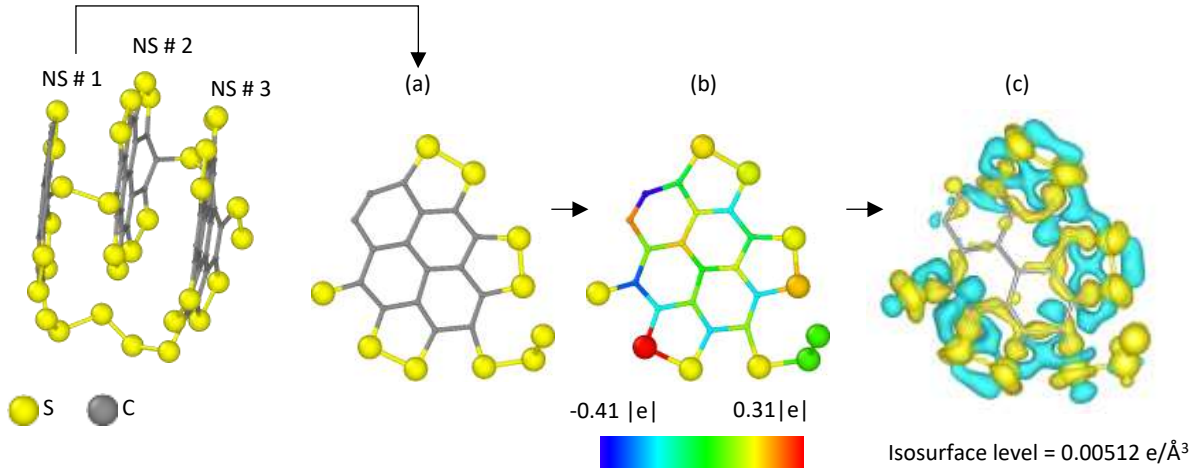

Figure 3: SC composite after eight ps AIMD simulation: (a) structure of graphene nanosheet labeled as NS # 1; (b) colored mapping of the Bader electronic charge distribution (see color bar), (c) charge energy difference. Cyan regions indicate a loss of charge, yellow regions a gain. DOL molecules not shown for clarity.

Electrochemical Lithiation Dynamics

After the AIMD stabilization of the SC/solvent system we proceeded to analyze the lithiation dynamics of the SC composite by randomly adding eight lithium atoms every eight ps nearby the lithiated SC composite (hereafter-called SC-Li composite).

Figure S1 (Supporting Information) shows the AIMD energy profile for an initial lithium loading of eight lithium atoms, equivalent to a 0.25:1 Li:S molar ratio. After 6 ps of simulation, the system stabilizes with no energy oscillations above 0.01 eV in the following two ps of simulation. Moreover, after eight ps the lithiated structure shows the Li atoms interacting preferentially with S atoms bonded to a C atom, with neither formation of long-chain Li PS nor Li PS dissolution into the liquid DOL phase, even though the low lithium contents. The absence of 8-membered ring sulfur structures before lithiation in the AIMD stabilized SC composite, plus the formation of *short-chain* Li PS at the at low lithium contents, suggest an electrochemical lithiation path alternative to the proposed *solid-liquid-solid* reaction path going from elemental sulfur to *long-chain* Li PS Li_2S_n ($4 < n < 8$) and then to Li_2S_2/Li_2S.[19, 44] This result agrees with earlier hypotheses on the absence of a two-step voltage plateaus during discharging of Li-S batteries based on SPAN composites or microporous carbonaceous materials, where sulfur is either suggested to be covalently bonded to the carbon backbone or confined into micrometric pore sizes in other forms different than S_8, respectively.[16, 45]

Figure 4 shows the principal axes of rotation of the SC-Li composite (0.25:1 Li:S molar ratio) calculated based on the weight distribution of the graphene nanosheets only. The structure alignment around the A_3 axis confirms the ordered stacking of the carbon backbone with the S and Li atoms surrounding it radially with no diffusion of either species into the space between nanosheets.

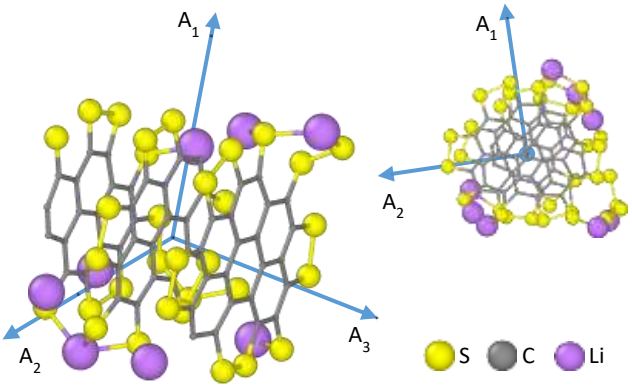

Figure 4: Principal axes of rotation of the SC composite at a Li/S molar ratio of 0.25.

Figure 5 shows the SC composite at increasing lithium contents up to a 2:1 Li:S molar ratio, with the principal axis of rotation A_3 pointing out of the paper in all cases. At lower than 1:1 Li:S molar ratios, the S reduction with Li takes place at the graphene nanosheets edges exclusively, with no significant disordering of the π-π stacking. However, at higher lithium contents the stacking disordering of the carbon backbone increases due to Li accumulation, with some Li atoms penetrating into the space between graphene nanosheets. Moreover, this is revealed by Figure 6 that plots the lithium and sulfur distribution around the A_3 axis at Li:S molar ratios of 0.25:1 and 2:1. Even though this Li accumulation lowers the carbon backbone stacking ordering, we observe that the sulfur reduction product keeps tightly attached to the carbon backbones with no formation of extended domains growing into the liquid phase. Formation of extended reduction products like Li_2S_2 and Li_2S is generally associated with irreversible capacity facing during battery cycling.[34]

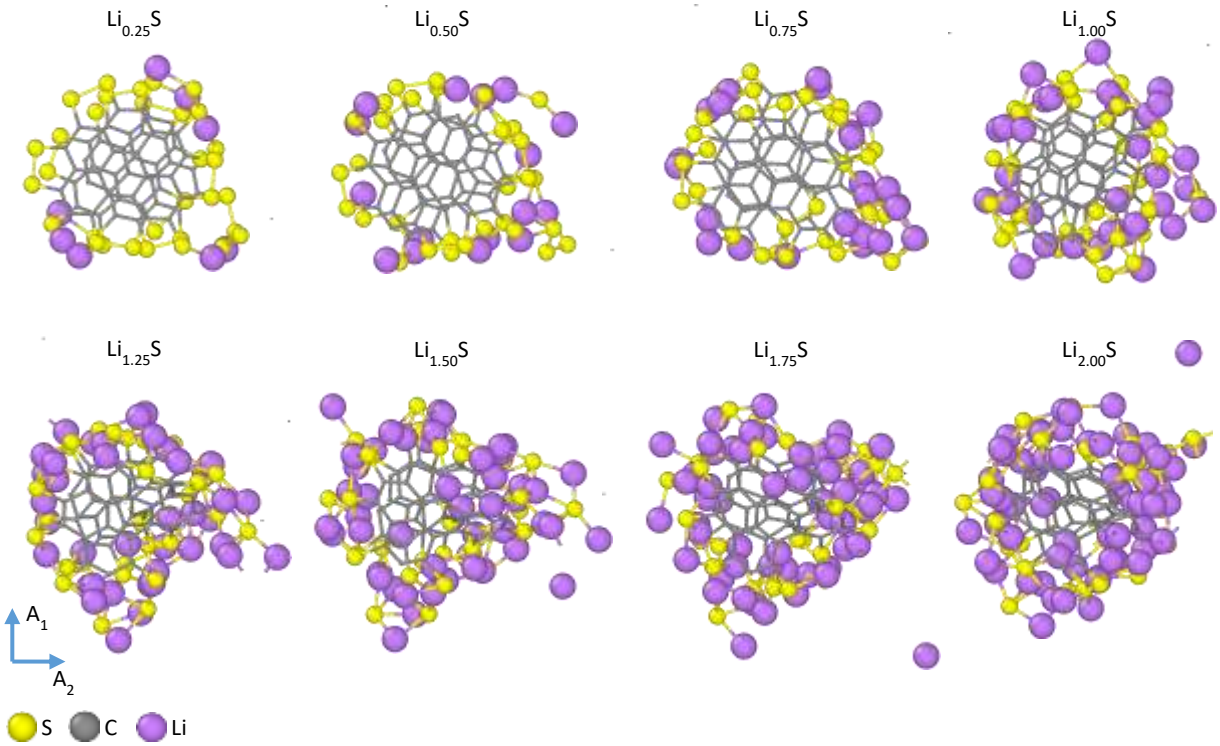

Figure 5: SC-Li composite structure with increasing lithium contents

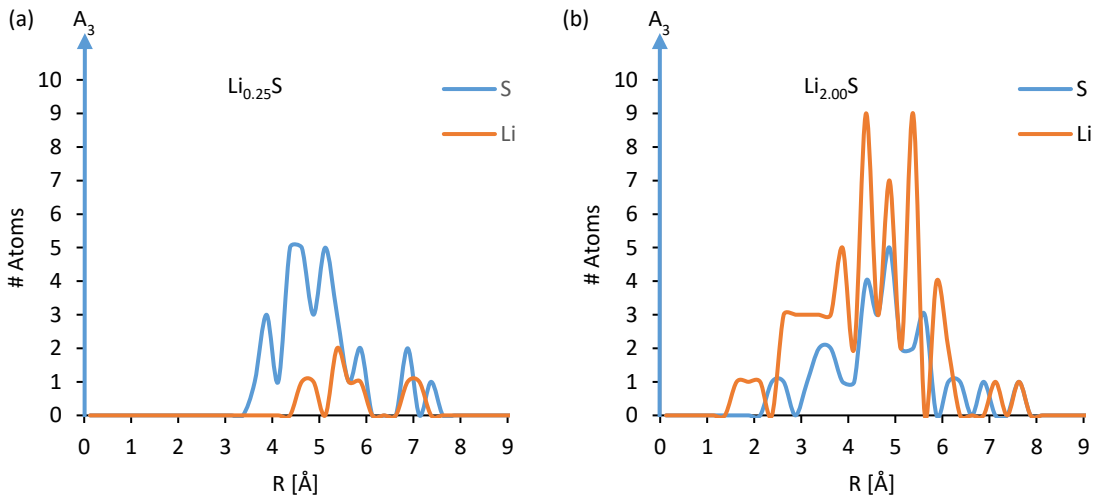

Figure 6: Lithium and sulfur distribution around the A_3 axis at (a) 0.25:1 and (b) 2:1 Li:S molar ratio

Figure 7 shows further structural insights for the SC composite at a 2:1 Li:S molar rate. Based on Equation 2, the electronic charge density difference between the SC composite and lithium atoms not only shows charge accumulation around the sulfur atoms but also between lithium and the carbon atoms located at the graphene edges.

The charge accumulation around sulfur is expected (Figure 7a), and it evidences the electrochemical reduction of sulfur, in agreement with the sulfur-sulfur RDF function (Figure 7b) showing no sulfur-sulfur

interactions shorter than 3 Å, suggesting no sulfur-sulfur bonding. The electron accumulation between lithium and carbon indicates possible bonding between the two species and explains the lithium accumulation close to the carbon backbone. On the other side, the lithium-oxygen RDF function (Figure 7b) shows an intense peak around 2 Å, indicating strong interactions between lithium and the oxygen atoms from the DOL solvent molecules.[21] The lithium interactions with carbon and oxygen suggest a competing effect between the carbon backbone and the liquid solvent in determining the morphology of sulfur reduction products. Earlier studies have reported the possible impact of the carbon backbone structure and the solvent properties, like the donor number and Li PS solubility, in minimizing the formation of insulating sulfur-containing films,[34] and eliminating the lithium PS shuttling during discharge.[16]

$$\Delta\rho = \rho_{\text{SC-Li composite}} - \rho_{\text{Graphene nanosheets/sulfur}} - \rho_{\text{Lithium}} \qquad \text{Eq. 2}$$

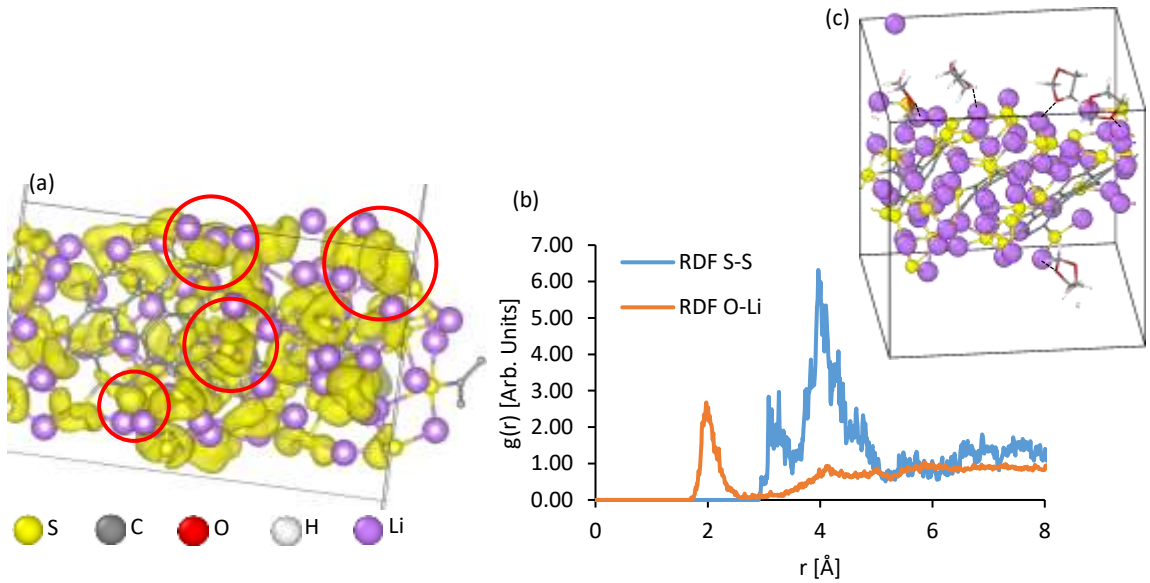

Figure 7: (a) charge density difference at 2:1 Li:S molar ratio: yellow regions indicate charge accumulation (some circled in red), charge depletion regions not shown for easier visualization. Isosurface level = 0.00498; (b) S-S and O-Li RDF functions; (c) SC-Li composite ($Li_{2.00}S$) / solvent interactions

The Bader charge analysis in Figure 8 shows no significant electronic exchange between the DOL solvent molecules and the SC-Li composite. It also reveals further insights on how the electrons distribute between the sulfur and carbon atoms during lithiation. The electrons coming into the cathode structure not only go to the sulfur atoms but also go into the carbon backbone, confirming the above charge difference analysis and suggesting the carbon backbone also reduces during the electrochemical lithiation process. The lithium-carbon interaction evidenced by both the charge density difference and the Bader charge analyses suggests an alternative reduction path where the carbon backbone not only improves the cathode electronic conductivity but also reduces during the electrochemical process.

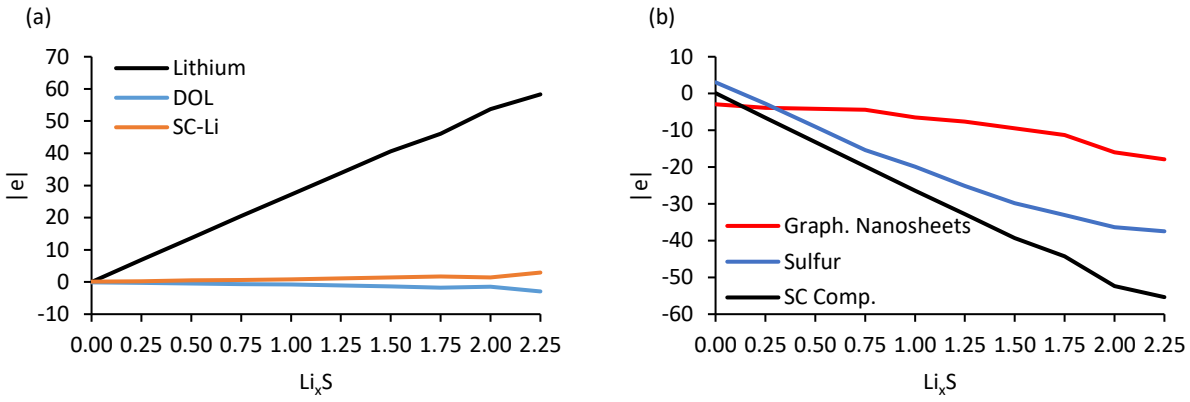

Figure 8: Total electron charge associated to (a) lithium atoms, DOL liquid phase, and lithiated SC composite, (b) electron charge distribution in the lithiated SC composite.

Figure 9 plots the coordination numbers for each sulfur atom with either carbon or lithium along with its corresponding Bader electron charge at Li:S molar ratios of 0:1, 2:1 and 2.25:1. We defined the carbon- and lithium-sulfur coordination cutoffs as 20% larger than the corresponding interaction peaks from the RDF analysis, allowing us to take into account possible structural distortions due to the π- π stacking of the carbon backbone. Before lithiation (0:1 Li:S), one out of 32 sulfur atoms (blue line) coordinates with two carbon atoms; 27 sulfur atoms coordinate with one carbon atom, and the four remaining sulfur atoms participate only in sulfur-sulfur bonding interactions without coordinating with any carbon atom. Moreover, the average Bader electronic charge associated with sulfur atoms is 0.095 |e| with no significant variation between two-, one-, or non-carbon coordinated sulfur atoms. After lithiation, at a 2:1 Li:S molar ratio, no sulfur atom coordinates with two carbon atoms, the number of one-carbon coordinated sulfur atoms (blue line) goes down to nineteen, and the number of non-carbon coordinated sulfur atoms goes up to thirteen. This behavior suggests that the sulfur reduction with lithium not only goes through sulfur-sulfur bond scissions but also induces partial cleaving of sulfur-carbon bonds, as suggested in earlier works on SPAN composites.[16]

In most cases the non-carbon coordinated sulfur atoms bear an average Bader electronic charge of -1.604 |e| and coordinate with 5 to 6 lithium atoms, whereas the one-carbon coordinated sulfur atoms coordinate with 3 to 4 lithium atoms with each sulfur atom getting an average Bader electron charge of -0.815 |e|. Even though we did not observe any sulfur atom coordinating with eight lithium atoms, as expected from crystalline Li_2S,[46] earlier works have also reported lowered sulfur-lithium coordination in nanometric Li_2S clusters.[47-48] The more negative electron charge in the non-coordinated sulfur atoms suggest earlier formation of Li_2S-like structures, compared to the one-coordinated sulfur atoms. The charge difference isosurfaces and Bader electron analysis discussed above suggest that the carbon backbone competes with sulfur in the electrochemical lithiation process, dragging electrons into its structure and accumulating lithium around it. We hypothesize that this behavior might allow the SC composite to accept lithium beyond a 2:1 Li:S molar ratio. To explore our assumption, we performed an AIMD simulation at a 2.25:1 Li:S molar ratio. Figure 9 (bottom) shows that the excess of lithium atoms induces further sulfur-carbon bond cleavage and enhances the sulfur coordination with lithium, with more sulfur atoms coordinating with six lithium atoms, and even one sulfur atom coordinating with seven lithium atoms, indicating that the SC-Li composite gets even closer to the formation of Li_2S-like structures as final reduction products.

Figure 10 shows the discharge voltage profile based on sulfur weight (ΔV vs. Li/Li^+) calculated with the Equation 3, which is a simple relationship based on the difference in chemical potentials between our SC-Li composite and metallic lithium. The Equation 3 also assumes negligible enthalpic and entropic contributions, and it is defined as the total energy change (ΔE_{total}) due to the Δx lithium insertion into the system, where $E_{bcc}(Li)$ corresponds to the energy per atom of crystalline body-centered cubic lithium.[49]

$$\Delta V = -[E_{total}(Li_{(x+\Delta x)}S_{32}C_{54})-[E_{total}(Li_xS_{32}C_{54})+\Delta x\ E_{bcc}(Li)]]/\ \Delta x \qquad \text{Eq. 3}$$

Figure 10 illustrates qualitative agreement between the calculated voltage and the experimental data, showing one voltage plateau around ~1.5 V with no significant differences between the two experimental curves even though the EC/DEC- and the DOL/DME-based mixtures used as electrolytes. The agreement between our results and the experimental data provides a first-principles-based confirmation to the hypotheses outlined in earlier works for the unusual single-plateau voltage discharge. The sulfur-carbon bonding prevents sulfur from retaining its cyclic S_8 structure, eliminates the formation of long-chain lithium PS during discharging and promotes an *all in-solid-state* sulfur reduction pathway with no dissolution of lithium PS into the liquid phase.

Moreover, we observe a positive voltage discharge of 1.41 V Li^+/Li at a 2.25:1 Li:S molar ratio, which indicates the SC-Li composite is thermodynamically favorable beyond a 2:1 Li:S molar ratio. This result provides a plausible explanation for the additional discharge capacity of 171 mhA/g above the theoretical value of 1672 mAh/g for the SPAN-based LiS battery with EC/DEC and the additional discharge capacity of 100 mhA/g for the case of the SPAN-based LiS battery with DOL/DME.[13, 16] The sulfur-carbon bonding improves the overall cathode electronic conductivity. It allows the electron transfer into the carbon backbone itself; favors lithiation processes beyond a 2:1 Li:S molar ratio by delaying the formation of Li_2S-like structures at low lithium contents, and promotes chemical retention of the sulfur reduction products even though the partial sulfur-carbon bond cleavage.

We believe that a stronger sulfur-carbon chemical bonding, as is also evidenced in sulfur cathodes based on graphitized polymers, might not only facilitate complete utilization of active sulfur during discharging, but also may eliminate the irreversible loss of active sulfur, and prevent the formation of extended Li_2S domains at the end of discharge. Further calculations will aim at elucidating the possibility of hidden reduction mechanisms during the electrochemical lithiation processes in SC composites based on nitrogen-dope multilayer graphene ensembles, to evaluate the effect of carbonate-based electrolytes on the sulfur reduction processes, and to studying possible recovering of sulfur-carbon chemical bonding upon charging.[16, 50]

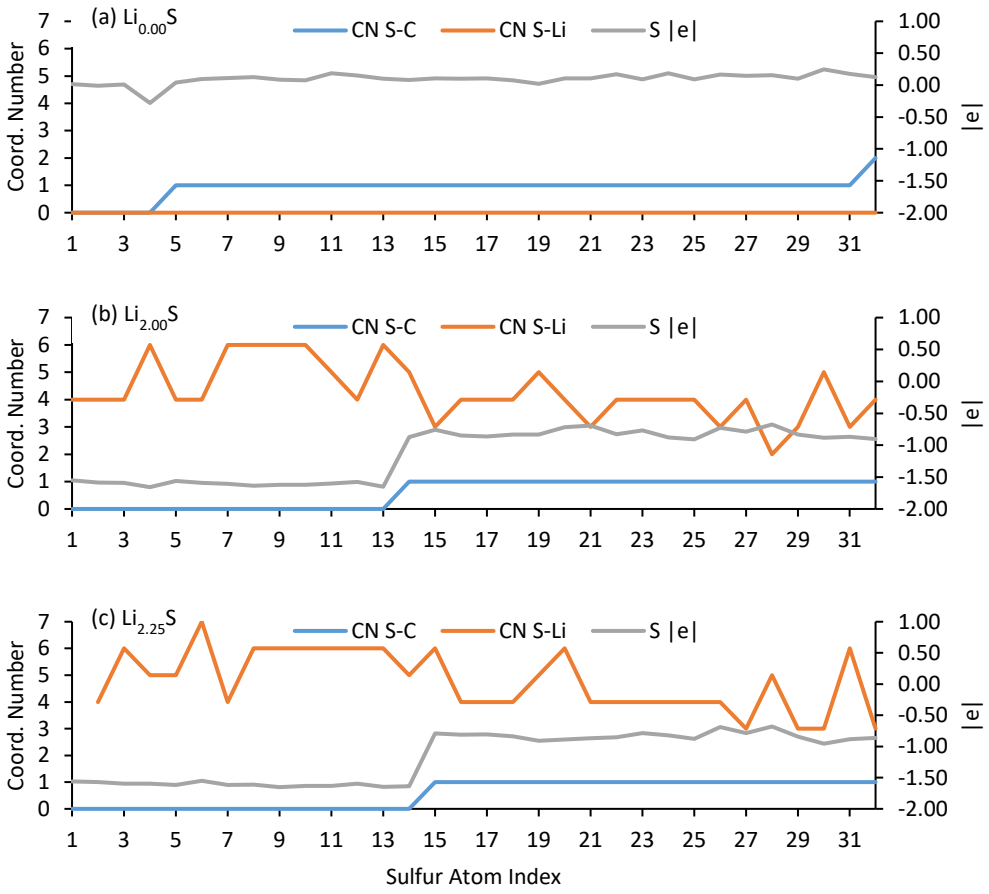

Figure 9: (left axis) sulfur-carbon coordination (CN S-C), sulfur-lithium coordination (CN S-Li), and (rigth axis) Bader electronic charge for each sulfur atom at (a) 0.25:1, (b) 2:1, and (c) 2.25:1 Li:S molar ratio

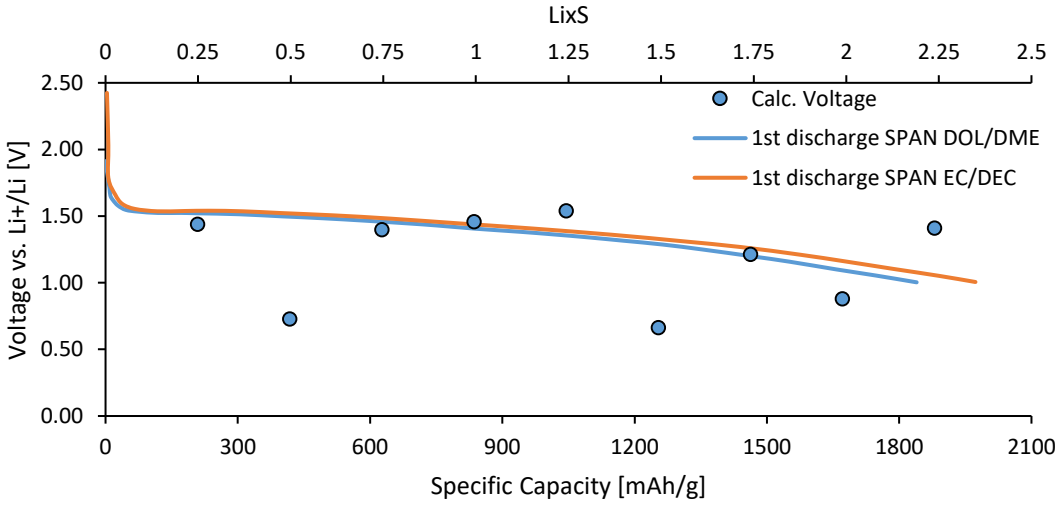

Figure 10: Voltage discharge profiles based on sulfur weight during sulfur reduction: voltage discharge calculated with Eq. 3 (Blue dots), voltage discharge for a SPAN Li-S battery with 1,3-dioxolane/dimethoxyethane (DOL/DME) as electrolyte (blue curve), voltage discharge for a SPAN Li-S battery with ethylencarbonate/diethylcarbonate (EC/DEC) as electrolyte.

Conclusions

The AIMD simulations performed in this work brought us to a more in-depth understanding of the electrochemical lithiation processes in a multilayer graphene nanosheet-based sulfur-carbon composite model (SC composite) embedded in a liquid DOL solvent phase, representative of a graphitized-polymer-based sulfur cathode. The results show that the sulfur-carbon chemical bonding in the SC composite prevents sulfur from retaining its stable cyclic S_8 structure, which leads to an electrochemical reduction path without formation of long-chain lithium polysulfides. The SC composite followed an *all in-solid-state* lithiation mechanism with both sulfur and carbon actively participating in the reduction process. The electrochemical lithiation dynamics promoted partial sulfur-carbon bond cleavage, with non-carbon-coordinated sulfur atoms coordinating with more lithium atoms than carbon-coordinated sulfur atoms. The calculated voltage discharge profile indicated that the SC composite lithiation is thermodynamically favorable beyond a 2:1 Li:S molar ratio, which provided a plausible explanation for the additional discharge capacity evidenced in earlier works with SPAN-based LiS batteries: the sulfur-carbon bonding improves the overall electronic conductivity, allowing the electronic transfer into the carbon backbone, and delaying the formation of Li_2S-like structures around the carbon-coordinated sulfur atoms.

Acknowledgements

This material is based upon work supported by the U.S. Department of Energy's Office of Energy Efficiency and Renewable Energy (EERE), as part of the Battery 500 Consortium, Award Number DE-EE0008210. This work was also supported in part by the Assistant Secretary for Energy Efficiency and Renewable Energy, Office of Vehicle Technologies of the U.S. Department of Energy under Contract No. DE-EE0006832 under the Advanced Battery Materials Research (BMR) Program. Supercomputer resources from Texas A&M University High Performance Computer Center and Texas Advanced Computing Center (TACC) are gratefully acknowledged.

References

1. Fang, R.; Zhao, S.; Sun, Z.; Wang, D. W.; Cheng, H. M.; Li, F., More Reliable Lithium-Sulfur Batteries: Status, Solutions and Prospects. *Adv. Mater.* **2017,** *29* (48), 1606823.
2. Manthiram, A.; Fu, Y.; Chung, S.-H.; Zu, C.; Su, Y.-S., Rechargeable Lithium–Sulfur Batteries. *Chem. Rev.* **2014,** *114* (23), 11751-11787.
3. Barghamadi, M.; Kapoor, A.; Wen, C., A Review on Li-S Batteries as a High Efficiency Rechargeable Lithium Battery. *J. Electrochem. Soc.* **2013,** *160* (8), A1256-A1263.
4. Warneke, S.; Eusterholz, M.; Zenn, R. K.; Hintennach, A.; Dinnebier, R. E.; Buchmeiser, M. R., Differences in Electrochemistry between Fibrous SPAN and Fibrous S/C Cathodes Relevant to Cycle Stability and Capacity. *J. Electrochem. Soc.* **2018,** *165* (1), A6017-A6020.
5. Fang, R.; Zhao, S.; Sun, Z.; Wang, D.-W.; Cheng, H.-M.; Li, F., More Reliable Lithium-Sulfur Batteries: Status, Solutions and Prospects. *Adv. Mater.* **2017,** *29* (48), 1606823.
6. Demir-Cakan, R., *Li-S Batteries: The Challenges, Chemistry, Materials and Future Perspectives*. World Scientific Publishing Europe Ltd.: 2017.
7. Yang, Y.; Zheng, G.; Cui, Y., Nanostructured sulfur cathodes. *Chem Soc Rev* **2013,** *42* (7), 3018-3032.
8. Zhou, W.; Xiao, X.; Cai, M.; Yang, L., Polydopamine-Coated, Nitrogen-Doped, Hollow Carbon–Sulfur Double-Layered Core–Shell Structure for Improving Lithium–Sulfur Batteries. *Nano Lett.* **2014,** *14* (9), 5250-5256.
9. Mosavati, N.; Chitturi, V. R.; Salley, S. O.; Ng, K. Y. S., Nanostructured titanium nitride as a novel cathode for high performance lithium/dissolved polysulfide batteries. *J. Power Sources* **2016,** *321*, 87-93.
10. Dysart, A. D.; Burgos, J. C.; Mistry, A.; Chen, C.-F.; Liu, Z.; Hong, C. N.; Balbuena, P. B.; Mukherjee, P. P.; Pol, V. G., Towards Next Generation Lithium-Sulfur Batteries: Non-Conventional Carbon Compartments/Sulfur Electrodes and Multi-Scale Analysis. *J. Electrochem. Soc.* **2016,** *163* (5), A730-A741.
11. Moon, S.; Jung, Y. H.; Jung, W. K.; Jung, D. S.; Choi, J. W.; Kim, D. K., Encapsulated Monoclinic Sulfur for Stable Cycling of Li–S Rechargeable Batteries. *Adv. Mater.* **2013,** *25* (45), 6547-6553.
12. Zhang, B.; Qin, X.; Li, G.; Gao, X., Enhancement of long stability of sulfur cathode by encapsulating sulfur into micropores of carbon spheres. *Energy Environ. Sci.* **2010,** *3* (10), 1531-1537.
13. Fanous, J.; Wegner, M.; Grimminger, J.; Andresen, Ä.; Buchmeiser, M. R., Structure-Related Electrochemistry of Sulfur-Poly(acrylonitrile) Composite Cathode Materials for Rechargeable Lithium Batteries. *Chem. Mater.* **2011,** *23* (22), 5024-5028.
14. Yin, L.; Wang, J.; Yang, J.; Nuli, Y., A novel pyrolyzed polyacrylonitrile-sulfur@MWCNT composite cathode material for high-rate rechargeable lithium/sulfur batteries. *J. Mater. Chem.* **2011,** *21* (19), 6807-6810.
15. Wei Seh, Z.; Li, W.; Cha, J. J.; Zheng, G.; Yang, Y.; McDowell, M. T.; Hsu, P.-C.; Cui, Y., Sulphur–TiO2 yolk–shell nanoarchitecture with internal void space for long-cycle lithium–sulphur batteries. *Nat. Commun.* **2013,** *4*, 1331.
16. Wei, S.; Ma, L.; Hendrickson, K. E.; Tu, Z.; Archer, L. A., Metal–Sulfur Battery Cathodes Based on PAN–Sulfur Composites. *J. Am. Chem. Soc.* **2015,** *137* (37), 12143-12152.
17. Yu, X.-g.; Xie, J.-y.; Yang, J.; Huang, H.-j.; Wang, K.; Wen, Z.-s., Lithium storage in conductive sulfur-containing polymers. *J. Electroanal. Chem.* **2004,** *573* (1), 121-128.
18. Yin, L.; Wang, J.; Lin, F.; Yang, J.; Nuli, Y., Polyacrylonitrile/graphene composite as a precursor to a sulfur-based cathode material for high-rate rechargeable Li-S batteries. *Energy Environ. Sci.* **2012,** *5* (5), 6966-6972.
19. Zhang, S. S., Liquid electrolyte lithium/sulfur battery: Fundamental chemistry, problems, and solutions. *J. Power Sources* **2013,** *231*, 153-162.

20. Warneke, S.; Zenn, R. K.; Lebherz, T.; Müller, K.; Hintennach, A.; Starke, U.; Dinnebier, R. E.; Buchmeiser, M. R., Hybrid Li/S Battery Based on Dimethyl Trisulfide and Sulfurized Poly(acrylonitrile). *Advanced Sustainable Systems* **2018,** *2* (2), 1700144.
21. Kamphaus, E. P.; Balbuena, P. B., First-Principles Investigation of Lithium Polysulfide Structure and Behavior in Solution. *J. Phys. Chem. C* **2017,** *121* (39), 21105-21117.
22. Grimme, S.; Antony, J.; Ehrlich, S.; Krieg, H., A consistent and accurate ab initio parametrization of density functional dispersion correction (DFT-D) for the 94 elements H-Pu. *J. Chem. Phys.* **2010,** *132* (15), 154104.
23. Becke, A. D.; Johnson, E. R., A density-functional model of the dispersion interaction. *J. Chem. Phys.* **2005,** *123* (15), 154101.
24. Tang, W.; Sanville, E.; Henkelman, G., A grid-based Bader analysis algorithm without lattice bias. *J. Phys.: Condens. Matter* **2009,** *21* (8), 084204.
25. Fujita, M.; Wakabayashi, K.; Nakada, K.; Kusakabe, K., Peculiar localized state at zigzag graphite edge. *J. Phys. Soc. Jpn.* **1996,** *65* (7), 1920-1923.
26. Magda, G. Z.; Jin, X. Z.; Hagymasi, I.; Vancso, P.; Osvath, Z.; Nemes-Incze, P.; Hwang, C. Y.; Biro, L. P.; Tapaszto, L., Room-temperature magnetic order on zigzag edges of narrow graphene nanoribbons. *Nature* **2014,** *514* (7524), 608-+.
27. Lei, Y. Y.; Jiang, W. R.; Dai, X.; Song, R. X.; Wang, B.; Gao, Y.; Wang, Z. G., Slippage in stacking of graphene nanofragments induced by spin polarization. *Sci Rep* **2015,** *5*, 4.
28. Perez Beltran, S.; Balbuena, P. B., Formation of Multi-layer Graphene Domains with Strong Sulfur-Carbon Interaction and Enhanced Sulfur Reduction Zones for Lithium-Sulfur Battery Cathodes. *ChemSusChem* **2018**.
29. Qin, Z.; Jung, G. S.; Kang, M. J.; Buehler, M. J., The mechanics and design of a lightweight three-dimensional graphene assembly. *Science Advances* **2017,** *3* (1).
30. Chen, Z.; Ren, W.; Gao, L.; Liu, B.; Pei, S.; Cheng, H.-M., Three-dimensional flexible and conductive interconnected graphene networks grown by chemical vapour deposition. *Nat. Mater.* **2011,** *10*, 424.
31. Mathioudakis, C.; Kelires, P. C., Modelling of Three-Dimensional Nanographene. *Nanoscale Research Letters* **2016,** *11* (1), 151.
32. Jang, B. Z.; Zhamu, A., Processing of nanographene platelets (NGPs) and NGP nanocomposites: a review. *Journal of Materials Science* **2008,** *43* (15), 5092-5101.
33. Safdari, M.; Al-Haik, M., Electrical conductivity of synergistically hybridized nanocomposites based on graphite nanoplatelets and carbon nanotubes. *Nanotechnology* **2012,** *23* (40), 405202.
34. Pan, H.; Chen, J.; Cao, R.; Murugesan, V.; Rajput, N. N.; Han, K. S.; Persson, K.; Estevez, L.; Engelhard, M. H.; Zhang, J.-G.; Mueller, K. T.; Cui, Y.; Shao, Y.; Liu, J., Non-encapsulation approach for high-performance Li–S batteries through controlled nucleation and growth. *Nat. Energy* **2017,** *2* (10), 813-820.
35. Ogoke, O.; Wu, G.; Wang, X.; Casimir, A.; Ma, L.; Wu, T.; Lu, J., Effective strategies for stabilizing sulfur for advanced lithium-sulfur batteries. *J. Mater. Chem. A* **2017,** *5* (2), 448-469.
36. Allen, M. J.; Tung, V. C.; Kaner, R. B., Honeycomb Carbon: A Review of Graphene. *Chem. Rev.* **2010,** *110* (1), 132-145.
37. Zu, C.; Li, L.; Qie, L.; Manthiram, A., Expandable-graphite-derived graphene for next-generation battery chemistries. *J. Power Sources* **2015,** *284*, 60-67.
38. Wen, Y.; He, K.; Zhu, Y.; Han, F.; Xu, Y.; Matsuda, I.; Ishii, Y.; Cumings, J.; Wang, C., Expanded graphite as superior anode for sodium-ion batteries. *Nat. Commun.* **2014,** *5*, 4033.
39. Wang, Y.-X.; Huang, L.; Sun, L.-C.; Xie, S.-Y.; Xu, G.-L.; Chen, S.-R.; Xu, Y.-F.; Li, J.-T.; Chou, S.-L.; Dou, S.-X., Facile synthesis of a interleaved expanded graphite-embedded sulphur nanocomposite as

cathode of Li–S batteries with excellent lithium storage performance. *J. Mater. Chem.* **2012,** *22* (11), 4744-4750.
40. Vijayakumar, M.; Govind, N.; Walter, E.; Burton, S. D.; Shukla, A.; Devaraj, A.; Xiao, J.; Liu, J.; Wang, C.; Karim, A., Molecular structure and stability of dissolved lithium polysulfide species. *Phys. Chem. Chem. Phys.* **2014,** *16* (22), 10923-10932.
41. Wang, L.; Zhang, T.; Yang, S.; Cheng, F.; Liang, J.; Chen, J., A quantum-chemical study on the discharge reaction mechanism of lithium-sulfur batteries. *J. Energy Chem.* **2013,** *22* (1), 72-77.
42. Mahmood, N.; Zhang, C.; Yin, H.; Hou, Y., Graphene-based nanocomposites for energy storage and conversion in lithium batteries, supercapacitors and fuel cells. *J. Mater. Chem. A* **2014,** *2* (1), 15-32.
43. Zheng, Y.; Li, H.; Yuan, H.; Fan, H.; Li, W.; Zhang, J., Understanding the anchoring effect of Graphene, BN, C2N and C3N4 monolayers for lithium−polysulfides in Li−S batteries. *Appl. Surf. Sci.* **2018,** *434* (Supplement C), 596-603.
44. Qie, L.; Zu, C.; Manthiram, A., A High Energy Lithium-Sulfur Battery with Ultrahigh-Loading Lithium Polysulfide Cathode and its Failure Mechanism. *Adv. Energy Mater.* **2016,** *6* (7), 1502459-n/a.
45. Xin, S.; Gu, L.; Zhao, N.-H.; Yin, Y.-X.; Zhou, L.-J.; Guo, Y.-G.; Wan, L.-J., Smaller Sulfur Molecules Promise Better Lithium–Sulfur Batteries. *J. Am. Chem. Soc.* **2012,** *134* (45), 18510-18513.
46. Park, H.; Koh, H. S.; Siegel, D. J., First-Principles Study of Redox End Members in Lithium–Sulfur Batteries. *J. Phys. Chem. C* **2015,** *119* (9), 4675-4683.
47. Liu, Z.; Deng, H.; Hu, W.; Gao, F.; Zhang, S.; Balbuena, P. B.; Mukherjee, P. P., Revealing Reaction Mechanisms of Nanoconfined Li2S: Implications for Lithium-Sulfur Batteries. *Phys. Chem. Chem. Phys.* **2018,** *20*, 11713-11721.
48. Yu, T.; Li, F.; Liu, C.; Zhang, S.; Xu, H.; Yang, G., Understanding the role of lithium sulfide clusters in lithium–sulfur batteries. *J. Mater. Chem. A* **2017,** *5* (19), 9293-9298.
49. Courtney, I. A.; Tse, J. S.; Mao, O.; Hafner, J.; Dahn, J. R., Ab initio calculation of the lithium-tin voltage profile. *Phys. Rev. B* **1998,** *58* (23), 15583-15588.
50. Jin, Z.-Q.; Liu, Y.-G.; Wang, W.-K.; Wang, A.-B.; Hu, B.-W.; Shen, M.; Gao, T.; Zhao, P.-C.; Yang, Y.-S., A new insight into the lithium storage mechanism of sulfurized polyacrylonitrile with no soluble intermediates. *Energy Storage Materials* **2018,** *14*, 272-278.

TOC Graphic